

Supporting Information

Rare Earth Double Perovskite for Underwater X-ray Imaging Applications

Ying Wang^{1,2#}, Chao Wang^{2#}, Luxuan Men², Jinlong Zhu², Qingsong Hu^{1,3}, Jiawen Xiao^{2*}, and Omar F. Mohammed^{3*}*

¹ Hubei Key Laboratory of Low Dimensional Optoelectronic Materials and Devices, Institute of Functional Materials, Hubei University of Arts and Science, Xiangyang 441053, China

² Beijing Key Lab of Microstructure and Property of Advanced Materials, College of Materials Science and Engineering, Beijing University of Technology, Beijing 100124, China

³ Advanced Membranes and Porous Materials Center (AMPMC) & KAUST Catalysis Center (KCC), Division of Physical Science and Engineering (PSE), King Abdullah University of Science and Technology (KAUST), Thuwal 23955-6900, Kingdom of Saudi Arabia

Corresponding Author: qingsong.hu@kaust.edu.sa, xiaojw@bjut.edu.cn,
omar.abdelsaboer@kaust.edu.sa

Experimental Section

Chemicals

Scandium chloride (ScCl_3 , 99.99%, RG, InnoChem), Yttrium chloride (YCl_3 , 99.9%, Bide Pharmatech Co., Ltd.), Lanthanum chloride hexahydrate ($\text{LaCl}_3 \cdot 6\text{H}_2\text{O}$, 99.9%, Bide Pharmatech Co., Ltd.), Cerium chloride heptahydrate ($\text{CeCl}_3 \cdot 7\text{H}_2\text{O}$, 95%, Bide Pharmatech Co., Ltd.), Praseodymium trichloride hexahydrate ($\text{PrCl}_3 \cdot 6\text{H}_2\text{O}$, 99.9%, Bide Pharmatech Co., Ltd.), Neodymium chloride hexahydrate ($\text{NdCl}_3 \cdot 6\text{H}_2\text{O}$, 99%, Bide Pharmatech Co., Ltd.), Samarium trichloride (SmCl_3 , 99%, Bide Pharmatech Co., Ltd.), Europium chloride hexahydrate ($\text{EuCl}_3 \cdot 6\text{H}_2\text{O}$, 98%, Bide Pharmatech Co., Ltd.), Gadolinium chloride (GdCl_3 , 99.95%, Bide Pharmatech Co., Ltd.), Terbium chloride (TbCl_3 , 97%, Bide Pharmatech Co., Ltd.), Dysprosium chloride (DyCl_3 , 99.9%, Shanghai Titan Scientific Co., Ltd.), Holmium chloride hexahydrate ($\text{HoCl}_3 \cdot 6\text{H}_2\text{O}$, 99%, Bide Pharmatech Co., Ltd.), Erbium chloride hexahydrate ($\text{ErCl}_3 \cdot 6\text{H}_2\text{O}$, 99.9%, Bide Pharmatech Co., Ltd.), Thulium chloride hexahydrate (TmCl_3 , 99.99%, Bide Pharmatech Co., Ltd.), Ytterbium chloride (YbCl_3 , 99.99%, Bide Pharmatech Co., Ltd.), Sodium chloride (NaCl , 99.9%, Beijing Honghu Lianhe Chemical Products Co., Ltd.), Cesium chloride (CsCl , 99%, Bide Pharmatech Co., Ltd.), Hydrochloric acid (HCl , 36.0-38.0%, China National Pharmaceutical Group Co., Ltd), Polydimethylsiloxane (PDMS, MARYDA MACHINERY CO., LIMITED), Curing agent (MARYDA MACHINERY CO., LIMITED). All reagents used in the experiments were used as received without further purification.

Synthesis

$\text{Cs}_2\text{NaLnCl}_6$ polycrystals-preparation method

Weighed 4 mmol of CsCl , 2 mmol of NaCl , and 2 mmol of LnCl_3 , and placed the raw materials into a 25 mL Teflon liner. Added 5 mL of hydrochloric acid, stirred the mixture for ten minutes, and then tightened the hydrothermal reactor

before inserting it into an intelligent temperature-controlled oven. The mixture was heated to 180 °C within 30 minutes and maintained at this temperature for 24 hours. Subsequently, it was cooled to room temperature at a cooling rate of 3 °C/min. The hydrothermal reactor was removed, and the crystals were washed with ethanol and dried at 60 °C for 24 hours to obtain Cs₂NaLnCl₆ polycrystals

Cs₂NaLnCl₆@PDMS scintillation screen preparation method

Weighed 2.0 g of PDMS and placed it in a glass bottle. Added 0.2 g of curing agent and then slowly added 0.4 g of Cs₂NaLnCl₆ powder, which had been passed through a 400-mesh sieve, to the PDMS while stirring vigorously. Stirring continued for 15 minutes, ensuring that the powder did not stick to the glassware during the addition process. The mixture was then vacuumed in a vacuum chamber for 30 minutes to remove air bubbles.

To produce a scintillator film with uniform thickness, the degassed mixture was dropped onto a glass plate and pressed with another glass plate of the same size. The film was subsequently heat-cured at 100 °C for 30 minutes, cooled to room temperature, and carefully removed from the surface of the glass plate to obtain a scintillation screen. To improve waterproof performance, more PDMS was added on the above resulted scintillation screen (by re-coating a PDMS layer), which significantly enhancing its water resistance compared with relative less PDMS coating, as shown in Figure S9. Consequently, all films discussed in the text refer to the film with more PDMS, and this will not be reiterated.

Instrumentation and characterizations

Phase, morphology, and chemical composition:

X-Ray powder diffraction (PXRD) patterns were collected at room temperature using a Bruker D8 advance diffractometer with Cu K α radiation ($\lambda = 1.5406 \text{ \AA}$)

at voltage = 40 kV, current = 40 mA. Phase purity analysis by comparing with the standard PDF card. Field emission scanning electron microscope (FSEM, Quanta650F) was used to observe the morphology of the powder, and obtain energy dispersive spectra (EDS). The chemical compositions on the surface of the sample were analyzed by EDS.

Photoluminescence performance:

The PL and PLE spectra were recorded by F-7000 fluorescence spectrometer to determine the emission and excitation wavelength. Photoluminescence quantum yield (PLQY) and time-resolved photoluminescence (TRPL) decay curves were measured using the steady-/transient- state fluorescence spectrometer FLS-1000 (Edinburgh Instruments), and the lifetime was calculated according to exponential fitting. The single exponential fitting formula is :

$$I = I_0 + A_1 * \exp\left(-\frac{x}{t_1}\right)$$

The double exponential fitting formula is :

$$I = I_0 + A_1 * \exp\left(-\frac{x}{t_1}\right) + A_2 * \exp\left(-\frac{x}{t_2}\right)$$

Where, I_0 is the original fluorescence intensity, A_1 and A_2 are the experimental results, t_1 and t_2 represent the fast decay process and slow decay process related to the quenching and radiation recombination of the luminescence center, respectively.

X-ray radioluminescence (RL) properties:

RL spectra were obtained by QE-Pro fluorescence spectrometer and Spectrum TEQ-PL system (Marine Optics) equipped with a fiber-coupled calibration integrating sphere. The X-ray tube (W target, TUB00153-9 series, MOXTEK) was used as the excitation source, and the radiation stability measurement was also done with this X-ray tube.

Determination of the detection limit:

The detection limit was assessed by quantifying the optical power of the scintillation light as follows. The scintillator was placed on a silicon-based optical power meter (843-R, Newport), and a copper foil was inserted to minimize the effect of transmitted X-ray photons on the power meter's response. The detection limit was determined using the signal-to-noise ratio (SNR) method. The X-ray dose was varied by fixing the voltage and increasing the current. The SNR was related to the reading of the optical power meter.

When the X-ray tube was turned off, the optical power meter read 0.01 nW, which was recorded as noise (SNR = 1) in a dark environment. Subsequently, the optical power of the light from the scintillator was measured at various X-ray dose rates. Then, the sample and power meter were removed, the dosimeter (Gold Diagnostic System, Radcal) was positioned in the same location as the sample, and the corresponding current and dose rate of the voltage were recorded. The detection limit of the scintillator was obtained when the SNR reached 3.

X-ray imaging:

The high-resolution images were taken with a commercial digital camera (SONY, ILCE-7RM2). The spatial resolution of scintillator X-ray imaging was evaluated using a test pattern plate (0.03 mm Pb, CN89729, made in Germany).

Determination of the light yield:

We estimated the light yields by using the commercial scintillators LYSO and BGO as references. After grinding the single crystal, weighed 0.5 g powder and press it into round wafer with a diameter of about 0.75 inch and a thickness of

2 mm to ensure full absorption of X-rays. The normalized RL spectrum of each reference and sample was calculated using

$$LY(\text{photons/MeV}) = \frac{\text{channel}_{BGO} \cdot \text{gain}_{sp} \cdot 1}{\text{channel}_{sp} \cdot \text{gain}_{BGO} \cdot EWQE} \cdot \frac{1}{0.662}$$

$$\frac{LY_{\text{sample}}}{LY_{\text{reference}}} = \frac{\eta_{\text{reference}} \int I_{\text{sample}}(\lambda) d\lambda \times S_{\text{reference}}}{\eta_{\text{sample}} \int I_{\text{reference}}(\lambda) d\lambda \times S_{\text{sample}}}$$

Where, channel represents the number of channels where the full-energy peak of the sample located. Gain represents the gain used in the test, and the gain value can only be determined by adjusting the position to make the full-energy peak appear completely. EWQE stands for emission-weighted quantum Efficiency. η is the percentage of X-ray deposition energy of the scintillator. I is the RL intensity at different λ (wavelength). S is the irradiation area, assuming that the X-ray intensity is uniform across the scintillator film. The $LY_{\text{reference}}$ represents LY_{LYSO} or LY_{BGO} .

The absolute light yield of the reference sample had been calibrated by pulse height spectroscopy, and the calibration data were about 10586 photons/MeV for BGO and 34463 photons/MeV for LYSO. To reduce the error in the measurement, 10000 photons/MeV was used for BGO and 33000 photons/MeV was used for LYSO.

Calculation of stretch limit:

A scintillator film with an initial length of 4.5 cm was captured. Fracture occurred when stretched to 9 cm (200% stretch). The stretch limit was calculated

according to the equation: $\text{Lim } \sigma = \frac{L_K - L_0}{L_0} \times 100\%$. Where, L_k is the tensile limit length and L_0 is the initial length.

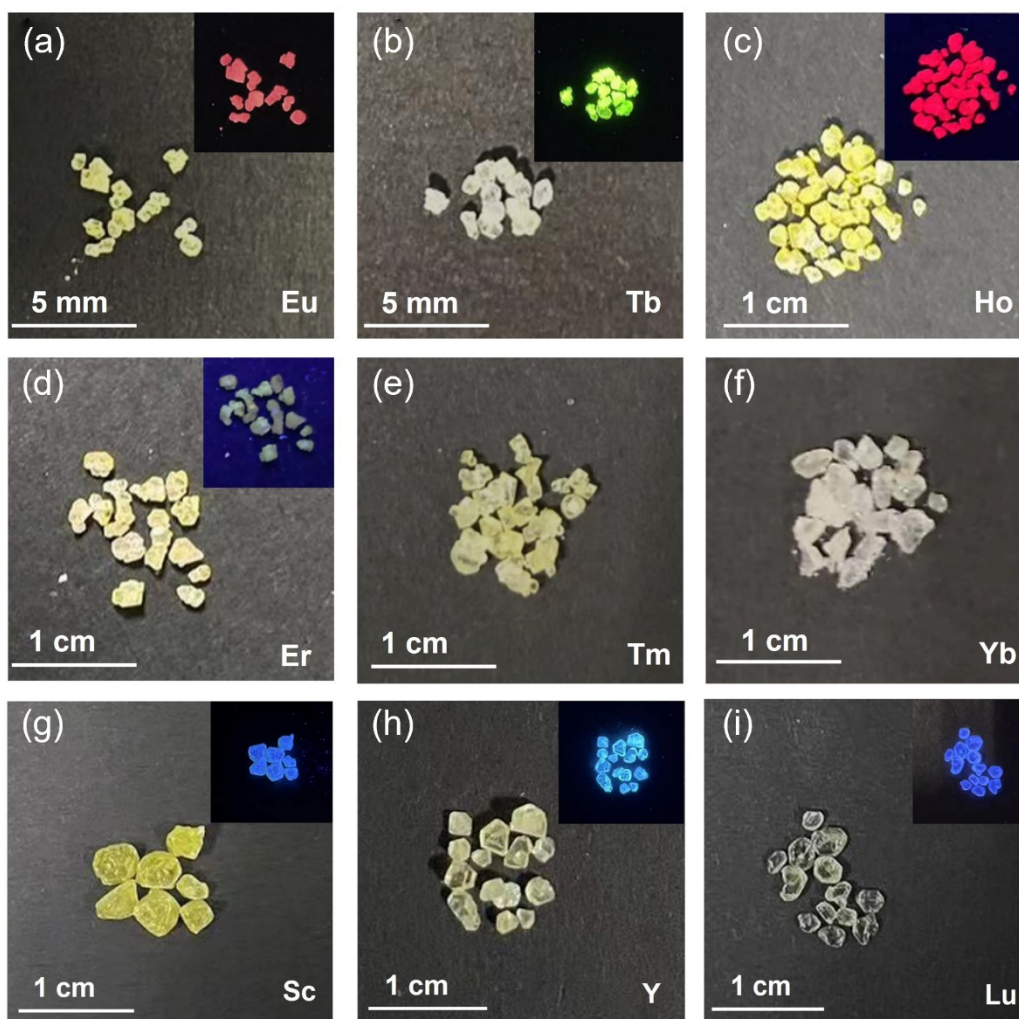


Figure S1. The photos of $\text{Cs}_2\text{NaLnCl}_6$ ($\text{Ln} = \text{Eu}, \text{Tb}, \text{Ho}, \text{Er}, \text{Tm}, \text{Yb}, \text{Sc}, \text{Y}, \text{Lu}$) under daylight and ultraviolet light.

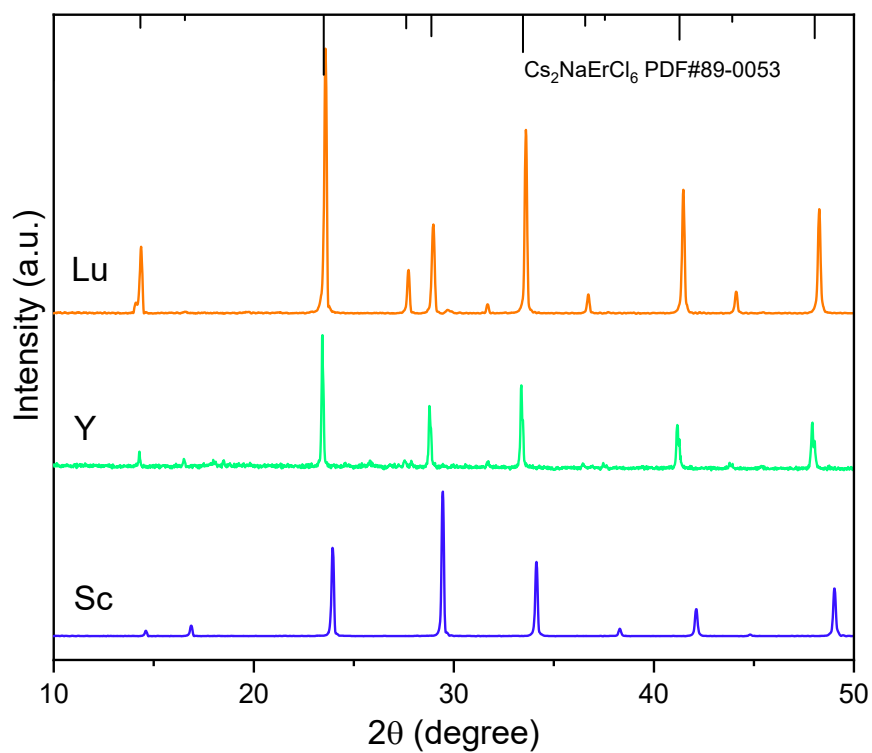


Figure S2. The PXRD of $\text{Cs}_2\text{NaLnCl}_6$ (Ln = Sc, Y, Lu) and the standard card date of $\text{Cs}_2\text{NaErCl}_6$ (PDF#89-0053).

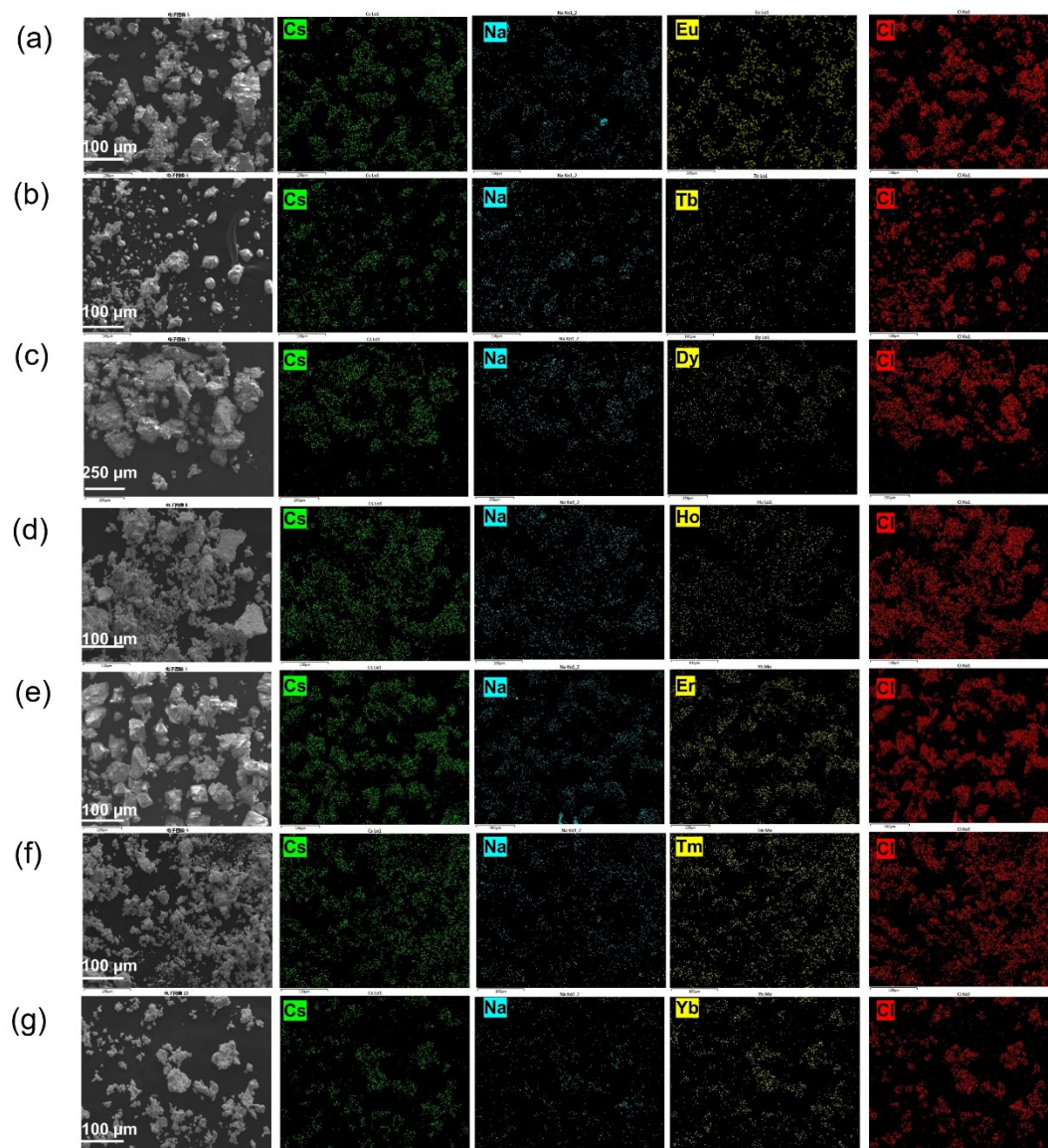


Figure S3. The energy dispersive spectrum (EDS) analysis of $\text{Cs}_2\text{NaLnCl}_6$ (Ln = Eu, Tb, Dy, Ho, Er, Tm, Yb) by field emission scanning electron microscopy (FESEM).

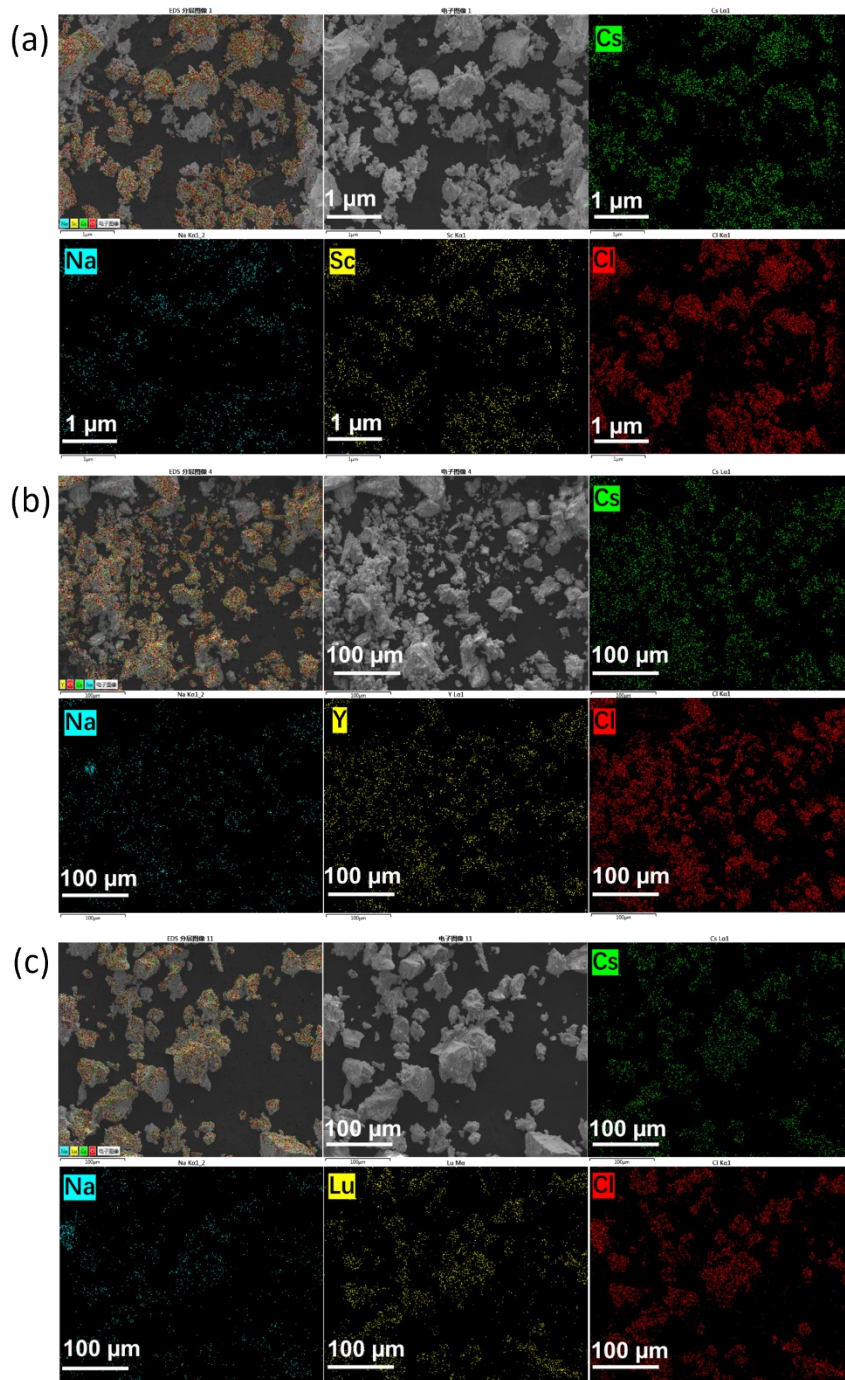


Figure S4. The energy dispersive spectrum (EDS) analysis of $\text{Cs}_2\text{NaLnCl}_6$ (Ln = Sc, Y, Lu) by FESEM.

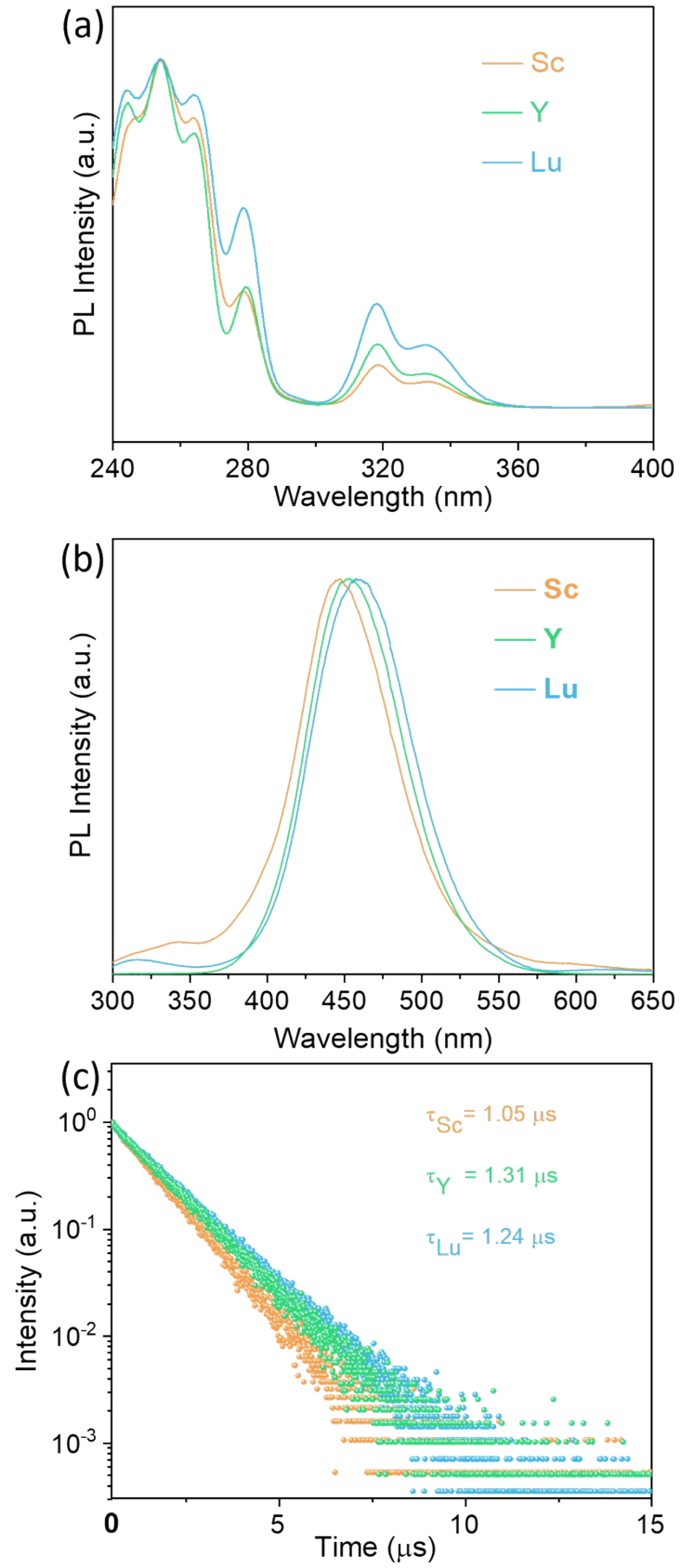


Figure S5. The PLE, PL, and lifetime curves of $\text{Cs}_2\text{NaLnCl}_6$ (Ln = Sc, Y, Lu).

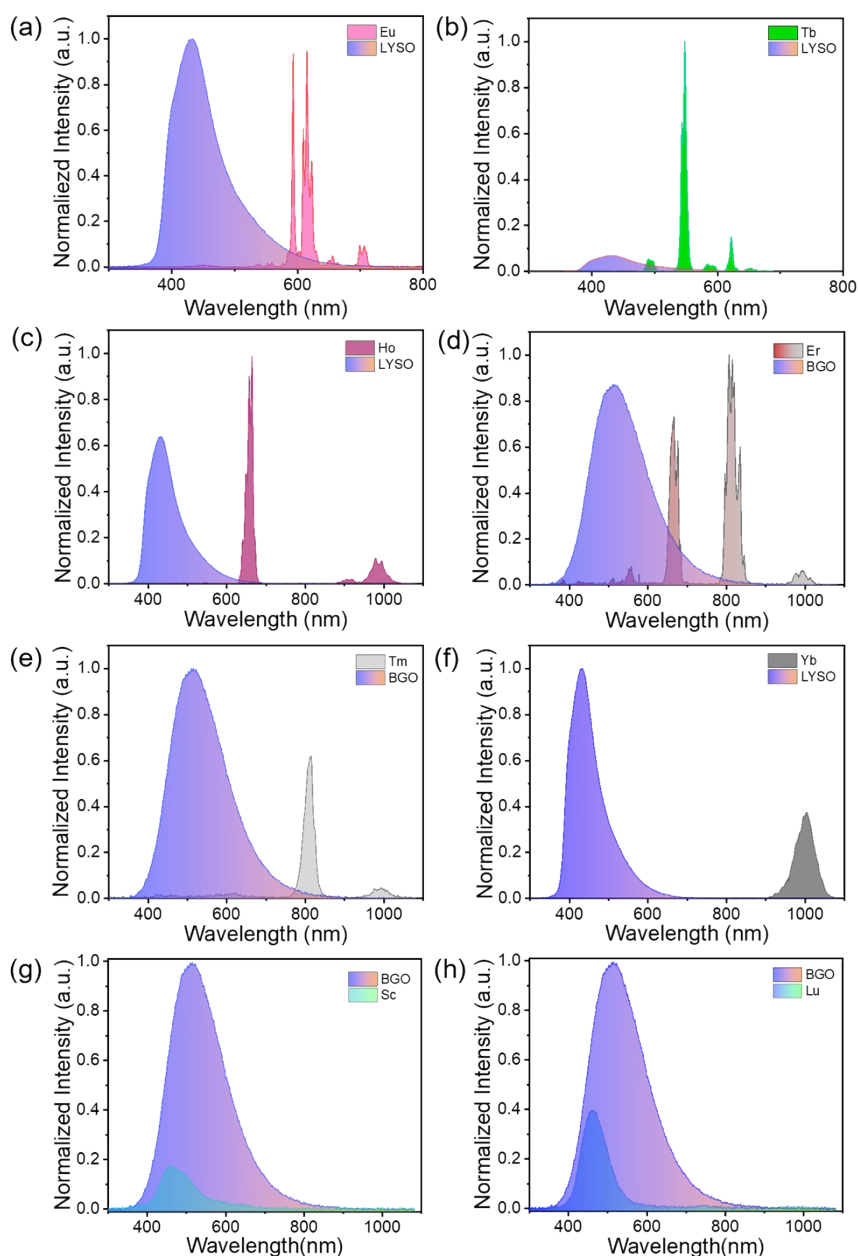


Figure S6. (a) The normalized radioluminescence (RL) spectra of $\text{Cs}_2\text{NaEuCl}_6$ and LYSO. (b) The normalized RL spectra of $\text{Cs}_2\text{NaTbCl}_6$ and LYSO. (c) The normalized RL spectra of $\text{Cs}_2\text{NaHoCl}_6$ and LYSO. (d) The normalized RL spectra of $\text{Cs}_2\text{NaErCl}_6$ and BGO. (e) The normalized RL spectra of $\text{Cs}_2\text{NaTmCl}_6$ and BGO. (f) The normalized RL spectra of $\text{Cs}_2\text{NaYbCl}_6$ and LYSO. (g) The normalized RL spectra of $\text{Cs}_2\text{NaScCl}_6$ and BGO. (h) The normalized RL spectra of $\text{Cs}_2\text{NaLuCl}_6$ and BGO.

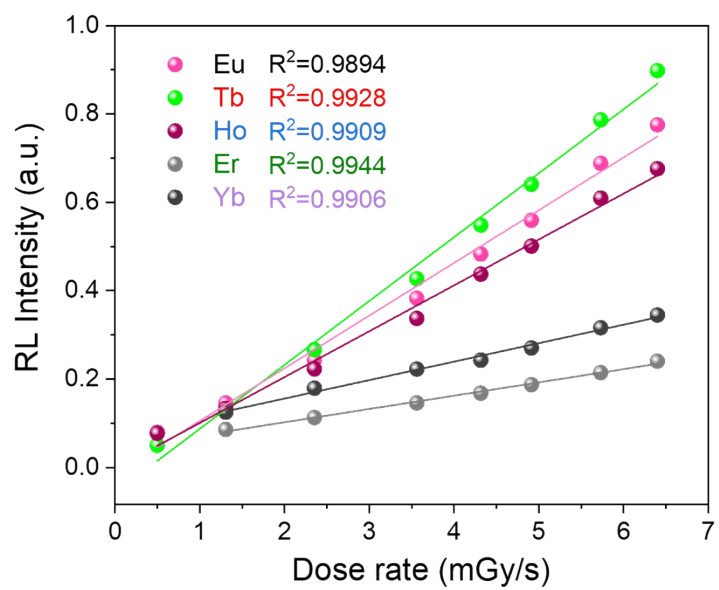


Figure S7. Dose dependence of the RL intensity of $\text{Cs}_2\text{NaLnCl}_6$ (Ln = Eu, Tb, Ho, Er, Yb).

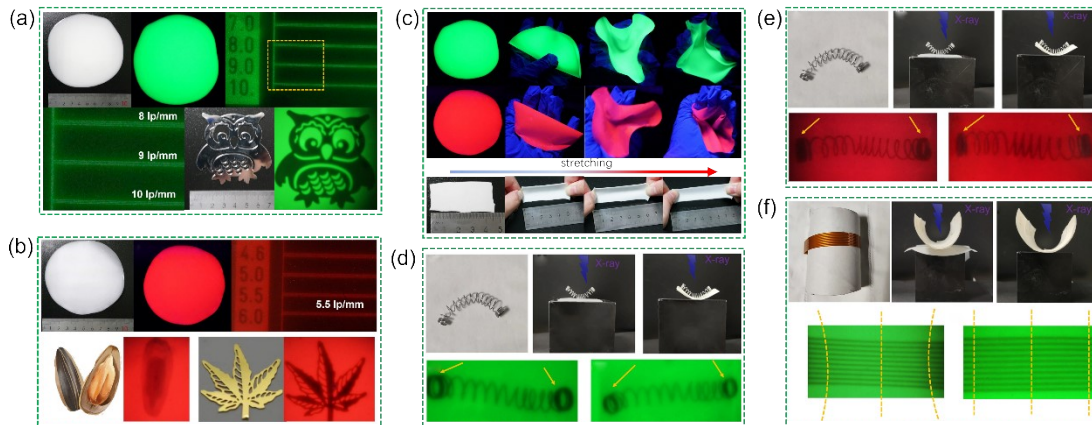


Figure. S8. (a) Photographs of $\text{Cs}_2\text{NaTbCl}_6@PDMS$ flexible film under daylight and UV lamp, spatial resolution, imaging device, and X-ray imaging photographs for the polymer film; (b) Photographs of $\text{Cs}_2\text{NaEuCl}_6@PDMS$ flexible film under daylight and UV lamp, spatial resolution, imaging device and X-ray imaging photographs for the polymer film. (c) Presentation of the performance of $\text{Cs}_2\text{NaLnCl}_6$ ($\text{Ln} = \text{Tb}, \text{Eu}$) @PDMS flexible film under various stress. The pictures and results of limit elongation test of the $\text{Cs}_2\text{NaTbCl}_6@PDMS$ flexible film. (d) Photographs of bent spring on the top of rigid and flexible $\text{Cs}_2\text{NaTbCl}_6@PDMS$ scintillation screens and X-ray images of rigid and flexible scintillation screens. (e) Photographs of bent spring on the top of rigid and flexible $\text{Cs}_2\text{NaEuCl}_6@PDMS$ scintillation screens and X-ray images of rigid and flexible scintillation screens. (f) Photographs of cylindrical circuit board on the top of rigid and flexible $\text{Cs}_2\text{NaTbCl}_6@PDMS$ scintillation screens, and X-ray imaging results of the cylindrical circuit board by rigid and flexible scintillation screens.

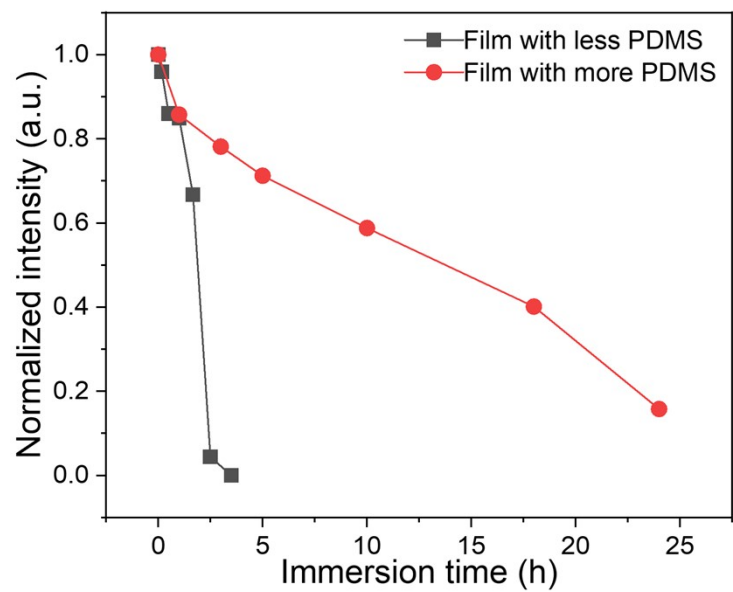


Figure S9. The normalized integrated intensity of the RL spectra of $\text{Cs}_2\text{NaTbCl}_6$ @PDMS film with less (black square dot plot) and more (red circular dot plot) PDMS in water at different times.

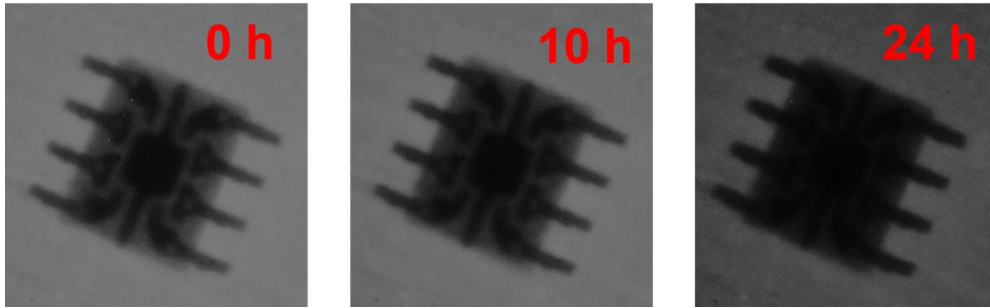


Figure S10. Underwater X-ray images of a chip using $\text{Cs}_2\text{NaTbCl}_6$ @PDMS flexible film at different times.

Table. S1 The atomic fraction of Cs₂NaLnCl₆ polycrystals

Material	Cs (%)	Na (%)	Ln (%)	Cl (%)
Cs ₂ NaScCl ₆	22.35	9.63	10.30	57.72
Cs ₂ NaYCl ₆	23.22	10.21	9.13	57.44
Cs ₂ NaEuCl ₆	21.73	11.50	10.79	55.98
Cs ₂ NaTbCl ₆	19.27	12.84	9.75	58.13
Cs ₂ NaDyCl ₆	19.62	10.16	12.83	57.40
Cs ₂ NaHoCl ₆	20.50	9.42	12.21	57.87
Cs ₂ NaErCl ₆	20.86	11.47	11.73	55.94
Cs ₂ NaTmCl ₆	22.00	10.57	11.42	56.01
Cs ₂ NaYbCl ₆	21.24	11.79	11.92	55.06
Cs ₂ NaLuCl ₆	21.03	12.29	11.14	55.55

Table. S2 Performance parameters of Cs₂NaLnCl₆ polycrystals

Material	Emission area	Excitation peak (nm)	Emission peak (nm)	Lifetime (ms)	Light yield (photons/MeV)	Stability (86 Gy)	Detection limit (nGy/s)
Cs ₂ NaEuCl ₆	visible	394	612	2.61	4400	95%	166.1
Cs ₂ NaTbCl ₆	visible	270	548	0.85, 6.31	42200	98%	67.8
Cs ₂ NaHoCl ₆	visible	462	657	2.04	9600	90%	85.5
Cs ₂ NaErCl ₆	visible	380	660	3.45	3300	95%	197.0
Cs ₂ NaTmCl ₆	near infrared	361	806	0.56	1400	/	/
Cs ₂ NaYbCl ₆	near infrared	287	996	2.73	6000	88%	170.7
Cs ₂ NaScCl ₆	visible	320	447	0.00105	1100	/	/
Cs ₂ NaYCl ₆	visible	320	454	0.00131	/	/	/
Cs ₂ NaLuCl ₆	visible	320	458	0.00124	1900	/	/